HHS Public Access

Author manuscript

Biomaterials. Author manuscript; available in PMC 2020 December 01.

Published in final edited form as:

Biomaterials. 2019 December ; 224: 119489. doi:10.1016/j.biomaterials.2019.119489.

Hydroxyapatite mineral enhances malignant potential in a tissue-engineered model of ductal carcinoma *in situ* (DCIS)

Frank He[1], **Nora L. Springer**[1,2], **Matthew A. Whitman**[1], **Siddharth P. Pathi**[1], **Yeonkyung Lee**[1], **Sunish Mohanan**[3], **Stephen Marcott**[1], **Aaron E. Chiou**[1], **Bryant S. Blank**[4], **Neil Iyengar**[5], **Patrick G. Morris**[5], **Maxine Jochelson**[6], **Clifford A. Hudis**[5], **Pragya Shah**[1,7], **Jennie A.M.R. Kunitake**[8], **Lara A. Estroff**[8,9], **Jan Lammerding**[1,7], **Claudia Fischbach**[1,9,*]

[1]Nancy E. and Peter C. Meinig School of Biomedical Engineering, Cornell University, Ithaca, NY, 14853, USA

[2]Department of Diagnostic Medicine/Pathobiology, Kansas State University College of Veterinary Medicine, Manhattan, KS, 66506, USA

[3]Department of Biomedical Sciences, Baker Institute for Animal Health, Cornell University, Ithaca, NY, 14853, USA

[4]Cornell Center for Animal Resources and Education, College of Veterinary Medicine, Cornell University, Ithaca, NY, 14853, USA

[5]Breast Medicine Service, Department of Medicine, Memorial Sloan Kettering Cancer Center/ Evelyn H. Lauder Breast and Imaging Center, New York, NY, 10065, USA

[6]Department of Radiology, Memorial Sloan Kettering Cancer Center/Evelyn H. Lauder Breast and Imaging Center, New York, NY, 10065, USA

[7]Weill Institute for Cell and Molecular Biology, Cornell University, Ithaca, NY, 14853, USA

[8]Department of Materials Science and Engineering, Cornell University, Ithaca, NY, 14853, USA

[9]Kavli Institute at Cornell for Nanoscale Science, Cornell University, Ithaca, NY, 14853, USA

Abstract

While ductal carcinoma *in situ* (DCIS) is known as a precursor lesion to most invasive breast carcinomas, the mechanisms underlying this transition remain enigmatic. DCIS is typically diagnosed by the mammographic detection of microcalcifications (MC). MCs consisting of non-stoichiometric hydroxyapatite (HA) mineral are frequently associated with malignant disease, yet

* cf99@cornell.edu.

Author Contributions: F.H. performed all experiments unless otherwise indicated. S.P.P., Y.L., S.M., and P.S. performed or assisted *in vitro* experiments. M.W., A.E.C., B.B., assisted *in vivo* experiments. N.S. and S.M. performed pathological diagnoses. N.I., P.G.M., M.J., and C.A.H. provided clinical samples. J.A.M.R.K. and L.A.E. analyzed the patient sample data. J.L. provided key reagents and tools. F.H. and C.F. designed the project and wrote the paper with input from S.P.P. All authors have approved the final article.

Competing Interests: The authors declare no competing interests.

Data availability: Data and materials are available upon request.

it is unclear whether HA can actively promote malignancy. To investigate this outstanding question, we compared phenotypic outcomes of breast cancer cells cultured in control or HA-containing poly(lactide-*co*-glycolide) (PLG) scaffolds. Exposure to HA mineral in scaffolds increased the expression of pro-tumorigenic interleukin-8 (IL-8) among transformed but not benign cells. Notably, MCF10DCIS.com cells cultured in HA scaffolds adopted morphological changes associated with increased invasiveness and exhibited increased motility that were dependent on IL-8 signaling. Moreover, MCF10DCIS.com xenografts in HA scaffolds displayed evidence of enhanced malignant progression relative to xenografts in control scaffolds. These experimental findings were supported by a pathological analysis of clinical DCIS specimens, which correlated the presence of MCs with increased IL-8 staining and ductal proliferation. Collectively, our work suggests that HA mineral may stimulate malignancy in preinvasive DCIS cells and validate PLG scaffolds as useful tools to study cell-mineral interactions.

Keywords

PLG scaffolds; ductal carcinoma *in situ*; hydroxyapatite; mammary microcalcifications; malignant progression

Introduction

Breast cancer is a leading cause of cancer-related deaths in women [1]. Breast tissue microcalcifications (MCs) serve as critical diagnostic indicators for non-palpable breast cancer during routine mammographic screening [2]. MCs are associated with 90-95% of all ductal carcinoma *in situ* (DCIS) cases as well as some high risk invasive cancers [3–6]. The presence of MCs in invasive ductal carcinoma (IDC) patients positively correlates with tumor aggressiveness as indicated by greater tumor volume, increased lymph node involvement, and decreased 8-year patient survival [7].

Despite their value as diagnostic markers, the functional relationship between MCs and breast cancer malignant progression remains unclear. Studies focused on MC chemical composition have found that MCs associated with benign breast lesions are exclusively composed of calcium oxalate while MCs associated with malignant breast lesions are largely composed of non-stoichiometric hydroxyapatite (HA) and related calcium phosphate minerals [4,5,8,9]. Although mammary MCs are currently treated as inert in clinical settings, *in vitro* studies have shown that HA is bioactive and can regulate breast cancer cell behavior [10–15]. In a recent study focused on breast tumor spheroids, the increased deposition of HA MCs within the viable cell regions correlated with cell line malignancy [16]. Collectively, these observations suggest that HA MCs may actively promote tumor progression and consequently, increase metastatic potential. The underlying mechanisms, however, remain unclear.

Both clinical and experimental studies suggest that DCIS is a precursor lesion to most invasive breast carcinomas (IBC) [17], though how DCIS progresses to IBC is a subject of much inquiry. Ductal breast cancer invasion into the surrounding stroma requires that tumor cells breach the basement membrane [18]. To facilitate their escape from the primary site, breast cancer cells are known to transition to a more mesenchymal phenotype [19] through a

dynamic, multifactorial process characterized by dysregulated proliferation, loss of cell-to-cell contact, and increased cell motility [18,20–22]. These properties are thought to be regulated by a network of cytokines in the tumor microenvironment [23–27]. In particular, interleukin-8 (IL-8) – which has been found to be enriched in neoplastic breast tissue [28,29] and in the circulation of advanced breast cancer patients [30] – may be critical for the induction and maintenance of a mesenchymal, de-differentiated phenotype [26,31] along with promoting increased breast cancer cell invasiveness [32,33]. Importantly, there is emerging evidence to suggest that IL-8 is upregulated in breast cancer cells interacting with HA mineral [13,14]. These studies, however, are limited by their focus on MDA-MB-231, a highly metastatic breast cancer cell line that is unsuitable for modeling the transition of preinvasive breast cancer to a more malignant phenotype.

Three-dimensional (3D) culture of breast cancer cells within poly(lactide-*co*-glycolide) (PLG) scaffolds can be used to recapitulate pathologically relevant tumor microenvironmental conditions [34,35]. When cultured within PLG scaffolds *in vitro*, cancer cells organize into tumor-like tissues that are representative of their *in vivo* counterparts, including comparable growth kinetics, cytokine secretion profiles, and formation of hypoxic cores [34]. Additionally, PLG scaffolds can be used to effectively present mineral to cells enabling studies of tumor cell-to-mineral interactions [13,14,36,37]. As such, HA-containing PLG scaffolds are well suited to study how mammary MCs may control breast cancer cell behavior. Here, this engineered 3D culture platform was employed to study breast cancer cell interactions with HA mineral *in vitro* and *in vivo*, with a particular focus on DCIS. Isogenic breast cancer cell lines of increasing malignancy were profiled for HA-mediated regulation of IL-8 secretion and cell proliferation. Morphological and migratory hallmarks of invasiveness were then assessed with a DCIS cell line cultured in HA scaffolds. Next, antibody inhibition studies were performed to test whether HA-mediated effects on DCIS cell motility were IL-8 dependent. Lastly, DCIS scaffold-xenografts were initiated in mice to assess the effects of HA-mineral on malignant tumor progression.

Materials and Methods

Cell lines and growth media

Human mammary epithelial cell lines from the MCF10A cell line series – MCF10A, MCF10DCIS.com, and MCF10CA1a (Karmanos Institute) – were cultured in 1:1 DMEM/F12 (Gibco) supplemented with 5% horse serum (Invitrogen), 1% penicillin/streptomycin (Gibco), 10 μg/ml insulin (Sigma), 0.5 μg/ml hydrocortisone (Sigma), 100 ng/ml cholera toxin (Sigma), and 20 ng/ml EGF (Millipore). Human mammary adenocarcinoma cell line MDA-MB-231 (ATCC) was cultured in DMEM (Gibco) supplemented with 10% FBS (Atlanta Biologicals) and 1% penicillin/streptomycin (Gibco).

Scaffold fabrication

Porous, polymeric scaffolds were fabricated using a gas-foaming, particulate leaching method [13]. For hydroxyapatite-containing (HA) scaffolds, poly(lactide-*co*-glycolide) (PLG) microparticles (ground and sieved, ~250 μm diameter; Lakeshore Biomaterials) and PLG microspheres (formed by double emulsion, ~5-50 μm diameter; Lakeshore

Biomaterials) were dry-mixed with nanocrystalline hydroxyapatite (Sigma #677418; phase-pure; stoichiometric; length 20-600 nm) and sodium chloride (sieved, ~250-400 μm diameter; J.T. Baker). The mixture was then pressed to form matrices (8.5 mm diameter, 1 mm thick) at room temperature in a dye press (Fred. S. Carver) and then pressurized in carbon dioxide (800 psi) with a non-stirred vessel (Parr Instruments). After a quick de-pressurization, scaffolds were soaked for 24 hours in de-ionized water to leach out the sodium chloride. Non-mineral-containing (PLG) scaffolds were fabricated similarly, excluding the hydroxyapatite in the starting mixture.

Three-dimensional cell culture

Scaffolds were sterilized in 70% ethanol for 20 minutes, washed multiple times with sterile PBS, then soaked in serum-containing media for 30 minutes. $1.5x10^6$ cells were statically seeded on each scaffold and then maintained under dynamic culture conditions on an orbital shaker. The scaffold-tumors were subjected to a 72-hour pre-culture period before analysis or additional *in vitro-based* studies. Gene expression analysis was performed after a 10-day culture period to increase cell numbers for analysis. For *in vivo* studies, scaffold-tumors were cultured for 24 hours prior to surgeries to enable sufficient cell adhesion and infiltration within the scaffold.

Scaffold characterization

To characterize mineralization, blank scaffolds were soaked in Alizarin Red S stain (20% of 40mM solution in de-ionized water, pH 4.1; VWR) for 20 minutes at room temperature and then washed 4 times in PBS. To visualize distribution of mineral throughout the porous scaffold matrix, blank scaffolds were scanned with a μCT system (Zeiss) and false-colored based on the attenuation coefficient (Avizo). To visualize cell associations with mineral in scaffolds, cell-seeded scaffolds were fixed in 4% paraformaldehyde (PFA) (VWR) overnight, embedded in paraffin blocks, cut into cross-sections, and subjected to von Kossa staining.

Analysis of cell proliferation and IL-8 expression

To assess proliferation, tumor cell-seeded scaffolds were lysed in Caron's buffer and sonicated at low power to liberate cellular DNA. Total DNA content was measured from these samples by the QuantiFluor® dsDNA System (Promega) according to manufacturer instructions. To quantify secretion of IL-8, tumor cell-seeded scaffolds were cultured in low serum prior to collection of media, which was then used in the IL-8 ELISA (R&D Systems) according to manufacturer instructions. To analyze IL-8 gene expression, total RNA was harvested from tumor cell-seeded scaffolds with TRIzol® (Invitrogen) according to manufacturer instructions and 1 μg was reverse transcribed to cDNA (qScript cDNA supermix, Quanta BioSciences). Quantitative real-time polymerase chain reaction (qRT-PCR) was performed using SYBR green detection (Quanta BioSciences) on an Applied Biosystems 7500 System. The following primer sequences were used: human IL-8 (fwd: 5'-agaaaccaccggaaggaaccatct-3', rev: 5'- agagctgcagaaatcaggaaggct-3') and human β-actin (fwd: 5' - aatgtggccgaggactttgattgc-3', rev: 5'- aggatggcaagggacttcctgtaa-3') (IDT Technologies). Quantitative analysis was performed based on the $\Delta\Delta C_t$ method [38]. Sample size was n = 3 or greater per condition.

Cell morphology and cell clustering analysis

Following an initial pre-culture period, MCF10DCIS.com cells were detached from scaffolds with 0.5% trypsin (Gibco) and re-seeded (4000 cells) onto glass coverslips (18 mm, #1 thickness; Karl Hecht) pre-coated with 30 μg/ml fibronectin (Gibco) (Fn). The re-seeded cells were maintained in standard culture conditions for either 4 hours to analyze single cell morphology or 24 hours to analyze cell colony characteristics, then fixed in 4% PFA, and co-stained for F-actin (1:100 Alexafluor 568 phalloidin; Invitrogen) and nuclei (1:2000 DAPI; Invitrogen). Imaging was performed on an epifluorescence microscope (Zeiss Observer Z1).

Morphology analysis of single cells was performed in ImageJ FIJI. Greyscale images were thresholded to create binary images and all single cells were analyzed for 1/circularity (perimeter^2 / 4*pi*area), which was termed ‘Morphology Factor’ (MF), and aspect ratio (major axis / minor axis) (AR). All measures of cell morphology were log-transformed to better fit the assumptions of the model (normality of residues, constant variance). The resulting data were analyzed using a mixed model with random (sample and nested replicates) and fixed (condition) effects. Sample size was n = 3 per condition and at least 30 cells were analyzed per sample. Graphs show the log-transformed MF and AR data.

Cell clusters were defined as cells that were tightly bound to at least one other cell. Sample size was n = 3 per condition; six representative images per sample were taken and manually counted for cells. The results were expressed as a percentage of the combined total of individual cells and clusters.

Cell motility analysis

To assess random cell migration, MCF10DCIS.com cells pre-cultured in scaffolds were detached with 0.5% trypsin (Gibco) and re-seeded (1500 cells) onto Fn-coated (Gibco) (30 μg/ml) optically clear 96-well plates for live cell tracking (IncuCyte) over 24 hours. IL-8 antibody (20 μg/ml; Cormorant Pharmaceuticals) was added to the media at the start of the experimental period. The x- y- movement of single cells were tracked over timeframes of 300 minutes. Sample size was n = 4 per condition and at least five cells were analyzed per sample.

To assess directed migration, MCF10DCIS.com cells pre-cultured in scaffolds were detached with 0.5% trypsin (Gibco) and re-seeded (5000 cells) into bovine collagen I-coated (40 μg/ml; Corning) transwells (8.0 μm pores; VWR) placed in 24-well plates. The cells were seeded in DMEM in the top chambers and induced to migrate towards bottom chambers containing DMEM 10% FBS over 16 hours. An IL-8 antibody (20 μg/ml; Cormorant Pharmaceuticals) was added to the DMEM in the top chamber at the start of the experimental period. Cotton swabs were used to carefully remove cells from the top sides of the transwell membranes. Cells were then fixed in 4% PFA and stained for nuclei (1:2000 DAPI; Invitrogen). A 2.5X objective was used to capture images that were later stitched together to show the entire transwell, which were then manually analyzed for migrated cells.

Human samples analysis

Sixteen patient samples – with mostly mixed pathologies of DCIS and Invasive Ductal Carcinoma (IDC) – were obtained for correlative histopathology and immunohistochemical (IHC) staining for IL-8. Tissue samples were transferred as frozen blocks from Memorial-Sloan Kettering Hospital using an approved IRB protocol. Frozen blocks were cryosectioned to 12 μm thickness and mounted on pre-cleaned glass slides. Prior to staining, sections were heated for 20 minutes at 65°C and re-hydrated in Tris-buffer. Sections were then blocked with 3% hydrogen peroxide to prevent signal interference from endogenous peroxidase activity. Antigen retrieval was performed with Proteinase K (Dako), and TNB solution (Perkin-Elmer) was used for blocking. Sections were incubated with primary antibody against IL-8 (5 μg/m; R&D Systems) overnight at 4°C, followed by a 30 min incubation at room temperature with a biotinylated secondary antibody against mouse (Vector Labs). To increase signal, the TSA amplification kit (Perkin-Elmer) was used according to manufacturer's direction. Signal detection was performed with DAB chromogen (Thermo Scientific), and sections were counter-stained with hematoxylin. Slides were then dehydrated via ethanol gradient and mounted with Entellan (Merck). Slides were scanned using the Aperio ScanScope System (Leica).

Scanned IL-8 IHC images were then transferred to a pathologist for specific evaluation and diagnosis. Slides were scored for gross intensity of IL-8 staining, and individual acini and ductal structures were identified for each slide and scored for ductal integrity/proliferative capacity as well as IL-8 stain intensity. Sections were comprehensively analyzed to identify all ductal structures, and all ductal structures were included in the analysis. If at least 3 ducts could not be identified, that particular section was not analyzed. All metrics were scored on a 0-to-3 scale, with 0 representing negligible intensity or proliferation and 3 representing maximal staining or excessive proliferation and total deterioration of acinar architecture. This analysis was performed blind, without knowledge of radiology or pathology reports from consulting clinicians. After full evaluation was completed, IHC evaluation was compared with radiology and pathology notes.

Scaffold-xenograft studies

Animal studies were conducted in accordance with Cornell University guidelines and were approved by Cornell University's Institutional Animal Care and Use Committee (IACUC). 6- to 7-week-old female Hsd:Athymic Nude-Foxn1^{nu} mice (n = 5 or 6) from Envigo were used for MCF10DCIS.com scaffold-xenograft studies. Scaffolds were seeded with 5×10^5 cells, maintained in dynamic culture conditions for 24 hours, and then kept on ice until implantation. Mice were anesthetized, and incisions were made to the dorsal interscapular skin. Contralateral subcutaneous pockets in the infrascapular regions containing the third pair of mammary glands were then gently enlarged using a sterile forcep, and then irrigated with sterile PBS. Cell-seeded scaffolds were then inserted into subcutaneous pockets, one on each side. The experimental endpoint was at 4 weeks. Scaffold-tumors were halved: one half was fixed in 4%PFA and embedded in paraffin while the other half was lysed with TPER buffer and mechanically/sonically digested. Blood was also collected and immediately processed to serum. IL-8 ELISA analysis (R&D Systems) was performed on both serum and tissue lysates.

The fixed and embedded scaffold-tumors were stained with hematoxylin and eosin (H&E) and Masson's Trichrome. Scanned images were then transferred to a board-certified pathologist for specific evaluation and diagnosis. Epithelial morphology, an assessment of ductal organization, was scored on a 1-to-4 scale, with 1 representing <25% fields containing organized tubules and acinar arrangements with central comedo and with 2, 3, and 4 representing 25-50%, 50-75%, and >75% fields with the aforementioned qualities, respectively. Fibrosis was scored on a 1-to-3 scale, with 1 representing thin distinct bands of fibrovascular stroma throughout sheets of neoplastic cells, and with 2 and 3 representing streaming thick fibrovascular bands separating neoplastic cells in <50% and >50% of fields, respectively. Cells with visible chromosomes were assessed as Mitotic Figures (ten 200x fields counted per sample). This analysis was performed blind.

Statistical analyses

For comparison between two conditions, unpaired Student's t and Mann-Whitney U tests were used to compare parametric and nonparametric data, respectively. For comparison between three conditions, ANOVA with Tukey's post hoc analyses were used to compare parametric data. A mixed model was used to analyze cell morphology data (see above). For *in vitro* studies, sample size was either n = 3 or 4, and at least two separate experiments were performed to confirm trends. Data are represented as means +/− SD and $p<0.05$ was considered statistically significant. GraphPad Prism 8 (GraphPad Software) and JMP 12 (SAS Institute) were used for statistical analyses, which were performed in consultation with an independent statistician from the Cornell Statistical Consulting Unit.

Results

Mineral-containing PLG scaffolds enable study of cell-mineral interactions in 3D

To investigate the effects of HA mineral on breast cancer cell behavior, we previously engineered a mineral-containing, scaffold-based culture platform [13,39]. The HA used in these scaffolds is commercially available, nanocrystalline HA, which we have thoroughly characterized by X-ray diffraction, IR spectroscopy, and transmission electron microscopy [14]. Here, we confirmed that these scaffolds enable direct interaction between HA mineral and the seeded cells. To test that mineral is available for cellular interactions, we soaked scaffolds in the calcium-chelating agent Alizarin Red S Stain (ARS). Indeed, mineral-containing but not control scaffolds exhibited strong red staining, indicating the surface presence of HA (Fig. 1A). Microcomputed tomography of scaffolds showed a homogeneous distribution of mineral throughout the porous matrix and comparable pore sizes between mineral-containing HA scaffolds and control PLG scaffolds (Fig. 1B), confirming previous results [13]. Breast cancer cells were statically seeded into the scaffolds and maintained in dynamic culture conditions (Fig. 1C) to promote oxygen and nutrient supply via convection, a process necessary to form tissue-like structures (Fig. 1D) in 3D. Von Kossa staining of cross-sections prepared from the seeded scaffolds showed that the cells attached along mineral-containing surfaces (Fig. 1D), which corroborated earlier work suggesting that breast cancer cells directly adhere to mineral-presenting substrates, including mineral-containing PLG scaffolds [13], mineral-coated surfaces [15], and mineralized collagen fibrils [40].

Correlation between IL-8 enrichment and the presence of MCs and proliferative ductal epithelia in clinical specimens

We had previously shown that interactions with HA mineral stimulate IL-8 secretion and proliferation in metastatic breast cancer cell lines *in vitro* [13–15]. To evaluate the clinical relevance of these findings to DCIS, we analyzed a set of human breast tissue samples with mostly mixed DCIS and invasive ductal carcinoma (IDC) pathologies. Microcalcifications were detected via mammography in over half of these patients and generally presented with morphologies that are linked with malignant lesions (Fig. 2A) [4]. IL-8 immunohistochemistry (IHC) showed variable staining patterns in all samples, with IL-8 present in ducts, stroma, or both (Fig. 2B). Pathological scoring revealed that IL-8 staining intensity was greater in samples with mammographically detected MCs (Fig. 2C), and within ducts, there appeared to be a positive correlation between ductal IL-8 staining intensity and ductal proliferation (Fig. 2D). Taken together, these analyses point to a potential link between the presence of mammographically-detected MCs in tumorigenic breast tissue and the upregulation of IL-8.

HA mineral regulates breast cancer cell proliferation and IL-8 secretion based on malignancy

To more directly investigate how the progression of breast cancer influences responses to HA mineral, we cultured three isogenically matched MCF10 cell lines – normal MCF10A (10A), premalignant MCF10DCIS.com (DCIS), and metastatic MCF10CA1a (CA1a) [41] – in mineral-containing scaffolds and used non-mineral-containing scaffolds as controls. We extracted nucleic acids from these scaffold-tumors to quantify cell growth using a DNA assay and IL-8 gene expression using qRT-PCR (Fig. 3A); we also quantified IL-8 secretion in the tumor-conditioned media using ELISA (Fig. 3A). We observed that HA stimulated proliferation in the normal (10A) and premalignant (DCIS) cell lines, but not in the invasive (CA1a) cells (Fig. 3B). Conversely, however, HA upregulated IL-8 gene expression (Fig. 3C) and soluble factor secretion (Fig. 3D) in the premalignant (DCIS) and metastatic (CA1a) cell lines, but not in the benign (10A) cells. Collectively, these data suggest that breast cancer cell exposure to HA mineral results in proliferation and IL-8 secretion responses dependent on malignant potential. Consistent with previous work, the detected differences in IL-8 secretion may be dependent on the engagement of the $\alpha v\beta 3$ integrin (Fig. S1) with proteins adsorbed onto HA mineral surfaces [42]. For the remainder of the study, we focused on the MCF10DCIS.com cell line, as they can form, in xenograft models, comedo-type lesions histopathologically representative of the high-grade DCIS in human samples [43]. Notably, this DCIS cell line exhibited a pronounced response to HA mineral, as both proliferation (Fig. 3B) and IL-8 expression (Fig. 3C, D) were increased, findings that are consistent with the histopathological analyses of human breast samples.

DCIS cells interacting with HA mineral in 3D culture adopt morphological hallmarks of invasiveness

As tumor cell malignancy is frequently accompanied by changes in morphology [44], we were next interested in whether breast cancer cell interactions with HA mineral could lead to altered morphological characteristics. To this end, DCIS cells were pre-cultured in either

mineral-containing or control scaffolds, trypsinized, and re-seeded onto Fn-coated glass coverslips for F-actin staining and imaging via epifluorescence microscopy (Fig. 4A). A tissue culture-treated polystyrene condition (2D) was included to control for effects of dimensionality and confirm that any observed effects were not due to enzymatic dissociation from scaffolds during the re-seeding process. Strikingly, DCIS cells pre-cultured in HA scaffolds adopted a wide variety of mesenchymal shapes associated with increased motility, including elongated spindles, dendritic stellates, and others [45,46] (Fig. 4B). We then quantified these changes by calculating, for each cell analyzed, a Morphology Factor (MF), which we determined to be effective at capturing motile cell shape diversity, especially when compared to the aspect ratio (Fig. S2). Indeed, we found that DCIS cells cultured in HA scaffolds exhibited a significant increase in MF when compared to ones pre-cultured in control PLG scaffolds (Fig. 4B, C). To assess how the formation of tumor cell colonies was impacted by prior exposure to HA mineral, we cultured the re-seeded DCIS cells for a total of 24 hours before imaging. We observed that HA appeared to promote hallmarks of invasiveness [47], including processes connecting multiple cell bodies and decreased cell-to-cell contact (Fig. 4D) when compared with PLG. Quantifying the relative number of cell clusters [48] confirmed a marked decrease in the percentage of cell clusters (and thus, an increase in the percentage of individual cells) in the DCIS cells pre-cultured in the HA scaffolds versus the control scaffolds (Fig. 4E). As expected, tumor cells pre-cultured in 3D exhibited significantly different behavior compared to their counterparts pre-cultured in 2D with regards to cell morphology and clustering. DCIS cells pre-cultured in 2D controls were generally rounder (Fig. 4B), and readily formed organized colonies with defined cell-to-cell junctions (Fig. 4D, E).

HA mineral increases DCIS cell motility through IL-8

Cells that adopt mesenchymal morphologies and exhibit increased individualization are associated with greater migratory potential [18,21,23]. Therefore, we then asked whether exposure to HA mineral in PLG scaffolds could increase the motility of DCIS cells. To this end, we performed live tracking of single DCIS cells that were pre-cultured in either mineral-containing or control scaffolds and then re-seeded onto Fn-coated optically-clear plates for analysis (Fig. 5A). A 2D condition was also included here to account for other experimental variables, as discussed above. We observed an increase in the random migration speed of DCIS cells pre-cultured in HA scaffolds versus control PLG scaffolds (Fig. 5B). Interestingly, a subset of HA pre-cultured DCIS cells also exhibited evidence of greater migratory persistence (Fig. 5C). To assess if the detected increase in HA-mediated motility was dependent on IL-8 signaling, we treated the pre-cultured cells with a function blocking IL-8 antibody at the start of the tracking period. Indeed, IL-8 inhibition decreased both migration speed and persistence in DCIS cells exposed to HA, but in contrast, no differences were observed in the control PLG scaffold condition with the same IL-8 antibody treatment (Fig. 5B, C). Moreover, we also found HA pre-cultured cells were responsive to IL-8 antibody treatment in a trans-well assay, supporting the role of IL-8 signaling on directed migration (Fig. S3). DCIS cells exhibited greater speed and persistence when pre-cultured in the 3D scaffold systems versus the 2D control (Fig. 5B, C), corresponding with the above-described changes of cell morphology associated with culture

dimensionality. Taken together, these data suggest that DCIS cells interacting with HA-mineral exhibit increased motility, an effect that could be regulated by IL-8 signaling.

Exposure of DCIS cells to HA mineral in scaffolds promotes features of increased malignancy in vivo

To assess the *in vivo* relevance of the above *in vitro* findings, we subcutaneously implanted DCIS cell-seeded HA mineral-containing and control PLG scaffolds into the contralateral infrascrapular regions containing the third pair of mammary glands of immunodeficient female nude mice. Scaffold-xenografts were harvested after 4 weeks and subjected to histopathological analyses (Fig. 6A). As expected, both HA and PLG scaffolds were largely degraded by the experimental endpoint (data not shown) [49]. In hematoxylin and eosin (H&E) stains of scaffold-xenograft cross sections, we observed that the PLG control scaffold tumors were typically composed of comedo-type lesions with relatively organized ductal structures (Fig. 6B, C), which is comparable to previous non-scaffold-based xenograft studies with the same MCF10DCIS.com cell line at this timepoint [43]. In contrast, H&E staining revealed significantly disorganized epithelial morphologies within the HA condition (Fig. 6B, C). Furthermore, Masson's trichrome staining revealed increased levels of fibrosis within HA scaffold-xenografts (Fig. 6D, E). DCIS xenografts initiated in HA scaffolds also showed greater mitotic activity versus DCIS xenografts initiated in PLG scaffolds (Fig. 6F). Interestingly, specimens that exhibited greater mitotic activity were also characterized by more fibrosis (Fig. 6G). To assess whether IL-8 could be upregulated by the presence of mineral *in vivo*, we also prepared tumor lysates and collected serum and performed ELISA-based cytokine detection. A subset of mice carrying HA-scaffold xenografts exhibited greater tumor and serum IL-8 relative to their PLG counterparts (Fig. 6H). There was a correlation between tumor and serum IL-8 concentrations within the HA but not the PLG condition (Fig. 6H). Taken together, these data suggest that HA mineral may regulate tumor malignancy *in vivo*, as evidenced by decreased epithelial organization, increased desmoplasia, and potentially enhanced IL-8 secretion. Importantly, the results from these scaffold-xenograft studies imply that our *in vitro* findings are relevant to *in vivo* scenarios and provide additional experimental evidence that HA-mineral could be actively promoting the malignant progression of breast cancer.

Discussion

Mammary MCs have been correlated with malignant progression in breast cancer but have thus far been primarily treated as passive indicators of cancer. In fact, the vast majority of DCIS cases present with MCs [3], and a recent study analyzing the chemical composition of human DCIS samples has confirmed that these malignant calcifications consist of non-stoichiometric HA [5]. Left untreated, between 14-53% of DCIS will progress to invasive breast cancer [50]. However, whether HA MCs can act as active microenvironmental triggers to induce malignant transformation is not clear. This work investigated the hypothesis that HA promotes phenotypic characteristics within DCIS lesions that facilitate the transition to a more malignant condition. By using a tissue-engineered culture model of DCIS to interrogate cell-mineral interactions both *in vitro* and *in vivo*, we found that HA mineral can

stimulate premalignant DCIS cells to develop invasive characteristics through a mechanism that may be dependent on IL-8 signaling.

Previous studies focused on bone metastasis have suggested that HA can stimulate secretions of various soluble factors in already aggressive breast cancer cells [13,14]. Here, we have observed that interactions with HA may also drive disease progression of DCIS by increasing IL-8 secretion. Our IHC analysis of human DCIS/IDC specimens correlates IL-8 enrichment with the presence of mammographic calcifications and proliferative ductal epithelium. *In vitro* studies using the HA scaffold system with a panel of different breast cancer cell lines further suggested that transformed cells may increase IL-8 secretion in response to HA regardless of their molecular profiles or subtypes. In contrast, non-transformed MCF10A cells did not exhibit increased IL-8 secretion in the HA-scaffolds, which raises the possibility that MCs may be pro-malignant but may not induce cancerous transformation without additional genetic or environmental drivers. Importantly, the increase in IL-8 secretion has been attributed to the inherent bioactivity of HA rather than stiffness differences between control and HA-containing PLG scaffolds [13]. A number of studies have pointed to a potentially crucial role for IL-8 in metastatic breast cancer, including enrichment of IL-8 in metastatic subpopulations of breast cancer cells [51–54] and high IL-8 levels observed clinically in patients with metastases [30]. Interestingly, enhanced IL-8 levels can stimulate invasion and metastasis via different mechanisms, for example, by promoting EMT via the overexpression of the transcription factor Brachyury [31] and by supporting angiogenesis [55,56], hypoxia response [34,56], and cancer stem cell regulation [52,57,58]. Future work will need to explore at more detailed molecular levels how exposure to HA mineral influences these various processes.

The observed HA-mediated increase of IL-8 secretion could be due to altered integrin engagement of breast cancer cells interacting with mineral versus control scaffolds. Integrins are cell adhesion receptors that govern intracellular signaling pathways [59] and can regulate the breast cancer metastatic phenotype [60]. Previous studies have shown that IL-8 secretion is linked to integrin-mediated cell adhesion [55,61], the dynamics of which are changed in mineralized cell culture systems due to differential protein adsorption onto mineral-containing surfaces [14,15]. Indeed, engagement of αvβ3 integrins contributed to IL-8 secretion by breast cancer cells exposed to mineral, as treatment with an αvβ3 function-blocking antibody inhibited this effect (Fig. S1). Interestingly, IL-8 itself can increase expression of αvβ3 [62,63], pointing to a possible positive feedback loop between HA-mediated αvβ3 integrin engagement and IL-8 expression. Although αvβ3 integrin expression levels have not been characterized in the MCF10 cell line series, integrin-mediated signaling events appear to play a more critical role in the transformed MCF10DCIS versus the non-transformed MCF10A cells [64]. Relative to MCF10A, MCF10DCIS cells possess high levels of the activated, phosphorylated forms of ERK and AKT [65], which are key to integrin-mediated signal transduction [59] that can stimulate the expression of chemokines such as IL-8 [66]. These studies suggest that an abundance of hyperactive signaling proteins essential to integrin-based signaling could explain the increased IL-8 expression in DCIS cells interacting with HA mineral in culture.

Additionally, HA-related changes in integrin engagement could be further regulated by the cell-surface glycoprotein CD44, which is a key mediator of cell-extracellular matrix (ECM) interactions [67]. In contrast to MCF10A, MCF10DCIS cells express the alternative isoform CD44v [65]. Interestingly, CD44v has been shown to promote integrin activation through engagement with osteopontin (OPN) [68], a secreted sialoprotein that is highly expressed in MCF10DCIS cells [16,69] and has a strong binding affinity for HA mineral [70]. Moreover, recent studies suggest that OPN is associated with increased breast cancer cell deposition of MCs and the capacity to metastasize [71,72]. As such, investigating the interplay between HA-OPN in the breast cancer microenvironment, tumor cell-surface CD44v, and integrin-mediated signaling pathways in future studies promises to reveal additional mechanistic insights.

The malignant transition of epithelial tumors is characterized by significant changes in tumor cell morphology [44], and previous studies have found that OSCC-3 cells – an aggressive, oral squamous cell carcinoma line – pre-cultured in PLG scaffolds exhibited less differentiated, fibroblastic morphology relative to those cultured in 2D [34]. Here we corroborated those findings with MCF10DCIS.com cells (Fig. 3B), and additionally observed that the incorporation of HA mineral into the scaffolds further advanced this trend, resulting in cell shapes associated with both mesenchymal and amoeboid morpho-phenotypes (Fig. 3B, S3) [73]. Carcinoma cells are known to rapidly switch between these phenotypic states when moving through a 3D matrix environment [74], and the significantly increased diversity of cell shapes (Fig. 3B, S3) that we observed following pre-culture in HA scaffolds could reflect an enhanced morphological plasticity mediated by mineral. We can speculate that the HA-mediated morpho-phenotypes may have imbued the tumor cells with additional modes of motility [74], as a subset of these cells exhibited more persistent movement (Fig. 4C). Invasive tumor cells can theoretically leverage multiple modes of motility to better respond to physical or biochemical changes in their environments [18]. Interestingly, these pre-cultured tumor cells still maintained 3D morphophenotypic characteristics during their re-seeded 2D culture periods. This observation supports the idea that HA-mediated changes in phenotypic state may in fact persist across multiple generations [75] and result in more invasive cell colonies even after initial exposure to HA mineral, which often presents heterogeneously in breast tissue [2].

Our studies here also implicate the potential role of IL-8 signaling in the HA-mediated increase in DCIS cell motility. Because our migration studies do not incorporate other cell types or additional soluble factors (Fig. 4, S3), we posit that these differences in motility were mediated through mechanisms that involve autocrine IL-8 signaling, which is essential for the maintenance of mesenchymal cell states [26] and has been shown to stimulate migratory behavior in both normal endothelial [76] and tumor [77,78] cells. Additional studies could further investigate how differences in breast cancer cell malignancy affect motogenic responses to IL-8 signaling. One could additionally consider the role of interleukin-6 (IL-6), as it has been recently shown to be working in concert with IL-8 to promote cell migration [79]. Although our studies focus exclusively on tumor cell interactions with mineral, future studies could investigate paracrine interactions between tumor cells and neighboring cell types within the context of a mineralized mammary microenvironment.

Microcalcifications are often found in the necrotic cores of breast tumors, likely occurring as a result of unregulated mineralization [5]. However, MC formation may also form via active, cell-mediated processes [80] that increase as a function of breast cancer malignancy [16]. More specifically, breast epithelial cells with mesenchymal characteristics may produce calcifications in a manner similar to osteoblasts during physiological bone formation and may be associated with the development of bone metastases [71,81]. Mammary tumors are also known to recruit pro-tumorigenic mesenchymal stem cells [82] that can spontaneously calcify [83,84]. Thus, we can speculate that the more malignant the tumor, the more likely that breast cancer cells within that tumor will be exposed to MCs. As we demonstrated in this study with a premalignant cell line model of DCIS, these increased cell-mineral interactions may further accelerate the progression of the malignant phenotype. More studies will be needed to assess how the physicochemical and materials properties of HA MCs in calcified breast tissue affect disease progression. Furthermore, DCIS are typically highly heterogeneous [85] with spatial variations in pathology, and thus cellular responses to HA MCs may not only differ across patients, but even within the same patient. In future work, performing a large-scale analysis of MC-containing tissue samples from controlled patient cohorts of DCIS and IDC will be essential to exploring how the physicochemical properties and microenvironmental context of HA MCs influences the progression of breast cancer. To experimentally assess functional connections and potential mechanisms, mineral-containing scaffolds could be re-engineered with specially-synthesized HA nanoparticles and employed in appropriate *in vitro* and *in vivo* setups.

Conclusions

Using a tissue-engineered model to study cell-mineral interactions in the breast tumor microenvironment, our data implies that HA mineral promotes invasiveness in a premalignant cell line model of DCIS. This study further validates the use of 3D polymeric scaffolds to study specific microenvironmental parameters that may enable progression towards increased tumor malignancy. Our work implicates HA calcifications as active promoters of malignancy in DCIS and supports the potential use of IL-8 as a prognostic biomarker for breast cancer malignant progression in patients with mammary MCs. Specifically, pathological analysis of MC and IL-8 co-localization may enable a more accurate prediction of whether a DCIS patient ultimately develops invasive breast carcinoma.

Supplementary Material

Refer to Web version on PubMed Central for supplementary material.

Acknowledgments

General: We thank Angela Du, Erica Feldman, Teresa Porri, Young Hye Song, and Matthew Tan for technical assistance; Joseph Druso and David Infanger for helpful discussions; and Francoise Vermeylen for statistical consultation.

Funding: This work was funded by National Cancer Institute Grants R01CA173083 and 1U54CA210184-01 and the Human Frontiers Science Program (RGP0016/2017). F.H. was supported by an NSF GRFP, an HHMI Med-into-Grad Fellowship, and a US Dept. of Education GAANN Fellowship. Additional imaging data was acquired through the Cornell University Biotechnology Resource Center, with NIH S10OD012287 funding.

References

[1]. Siegel RL, Miller KD, Jemal A, Cancer statistics, 2018, CA. Cancer J. Clin 68 (2018) 7–30. doi: 10.3322/caac.21442.

[2]. Wilkinson L, Thomas V, Sharma N, Microcalcification on mammography: Approaches to interpretation and biopsy, Br. J. Radiol 90 (2017). doi:10.1259/bjr.20160594.

[3]. Hofvind S, Iversen BF, Eriksen L, Styr BM, Kjellevold K, Kurz KD, Mammographic morphology and distribution of calcifications in ductal carcinoma in situ diagnosed in organized screening, Acta Radiol. 52 (2011) 481–487. doi:10.1258/ar.2011.100357. [PubMed: 21498306]

[4]. Tse GM, Tan PH, Cheung HS, Chu WCW, Lam WWM, Intermediate to highly suspicious calcification in breast lesions: A radio-pathologic correlation, Breast Cancer Res. Treat 110 (2008) 1–7. doi:10.1007/s10549-007-9695-4. [PubMed: 17674189]

[5]. Kunitake JAMR, Choi S, Nguyen KX, Lee MM, He F, Sudilovsky D, Morris PG, Jochelson MS, Hudis CA, Muller DA, Fratzl P, Fischbach C, Masic A, Estroff LA, Correlative imaging reveals physiochemical heterogeneity of microcalcifications in human breast carcinomas, J. Struct. Biol 202 (2018) 25–34. doi:10.1016/j.jsb.2017.12.002. [PubMed: 29221896]

[6]. Boughey JC, Gonzalez RJ, Bonner E, Kuerer HM, Current Treatment and Clinical Trial Developments for Ductal Carcinoma In Situ of the Breast, Oncologist. 12 (2007) 1276–1287. doi:10.1634/theoncologist.12-11-1276. [PubMed: 18055847]

[7]. Ling H, Bin Liu Z, Xu LH, Xu XL, Liu GY, Shao ZM, Malignant calcification is an important unfavorable prognostic factor in primary invasive breast cancer, Asia. Pac. J. Clin. Oncol 9 (2013) 139–145. doi:10.1111/j.1743-7563.2012.01572.x. [PubMed: 22897789]

[8]. Haka AS, Shafer-peltier KE, Fitzmaurice M, Crowe J, Dasari RR, Feld MS, Identifying Microcalcifications in Benign and Malignant Breast Lesions by Probing Differences in Their Chemical Composition Using Raman Spectroscopy Identifying Microcalcifications in Benign and Malignant Breast Lesions by Probing Differences in Their Che, (2002) 5375–5380.

[9]. Scott R, Stone N, Kendall C, Geraki K, Rogers K, Relationships between pathology and crystal structure in breast calcifications: an in situ X-ray diffraction study in histological sections, Npj Breast Cancer. 2 (2016) 16029. doi:10.1038/npjbcancer.2016.29. [PubMed: 28721386]

[10]. Wang Y, Yu X, Baker C, Murphy WL, McDevitt TC, Mineral particles modulate osteo-chondrogenic differentiation of embryonic stem cell aggregates, Acta Biomater. 29 (2016) 42–51. doi:10.1016/j.actbio.2015.10.039. [PubMed: 26597546]

[11]. Morgan MP, Cooke MM, Christopherson PA, Westfall PR, McCarthy GM, Calcium hydroxyapatite promotes mitogenesis and matrix metalloproteinase expression in human breast cancer cell lines, Mol. Carcinog 32 (2001) 111–117. doi:10.1002/mc.1070. [PubMed: 11746823]

[12]. Cox RF, Hernandez-Santana A, Ramdass S, McMahon G, Harmey JH, Morgan MP, Microcalcifications in breast cancer: Novel insights into the molecular mechanism and functional consequence of mammary mineralisation, Br. J. Cancer 106 (2012) 525–537. doi:10.1038/bjc.2011.583. [PubMed: 22233923]

[13]. Pathi SP, Kowalczewski C, Tadipatri R, Fischbach C, A novel 3-D mineralized tumor model to study breast cancer bone metastasis, PLoS One. 5 (2010) 1–10. doi:10.1371/journal.pone.0008849.

[14]. Pathi SP, Lin DDW, Dorvee JR, Estroff LA, Fischbach C, Hydroxyapatite nanoparticle-containing scaffolds for the study of breast cancer bone metastasis, Biomaterials. 32 (2011) 5112–5122. doi:10.1016/j.biomaterials.2011.03.055. [PubMed: 21507478]

[15]. Choi S, Coonrod S, Estroff L, Fischbach C, Chemical and physical properties of carbonated hydroxyapatite affect breast cancer cell behavior, Acta Biomater. 24 (2015) 333–342. doi:10.1016/j.actbio.2015.06.001. [PubMed: 26072364]

[16]. Vidavsky N, Kunitake JA, Chiou AE, Northrup PA, Porri TJ, Ling L, Fischbach C, Estroff LA, Studying biomineralization pathways in a 3D culture model of breast cancer microcalcifications, Biomaterials. 179 (2018) 71–82. doi:10.1016/j.biomaterials.2018.06.030. [PubMed: 29980076]

[17]. Espina V, Liotta LA, What is the malignant nature of human ductal carcinoma in situ?, Nat. Rev. Cancer 11 (2011) 68–75. doi:10.1038/nrc2950. [PubMed: 21150936]

[18]. McSherry EA, Donatello S, Hopkins AM, McDonnell S, Molecular basis of invasion in breast cancer, Cell. Mol. Life Sci 64 (2007) 3201–3218. doi:10.1007/s00018-007-7388-0. [PubMed: 17957337]

[19]. Choi Y, Lee HJ, Jang MH, Gwak JM, Lee KS, Kim EJ, Kim HJ, Lee HE, Park SY, Epithelial-mesenchymal transition increases during the progression of in situ to invasive basal-like breast cancer, Hum. Pathol 44 (2013) 2581–2589. doi:10.1016/j.humpath.2013.07.003. [PubMed: 24055090]

[20]. Thiery JP, Epithelial–mesenchymal transitions in tumour progression, Nat. Rev. Cancer 2 (2002) 442–454. doi:10.1038/nrc822. [PubMed: 12189386]

[21]. Polyak K, Weinberg RA, Transitions between epithelial and mesenchymal states: Acquisition of malignant and stem cell traits, Nat. Rev. Cancer 9 (2009) 265–273. doi:10.1038/nrc2620. [PubMed: 19262571]

[22]. Shibue T, Weinberg RA, EMT, CSCs, and drug resistance: The mechanistic link and clinical implications, Nat. Rev. Clin. Oncol 14 (2017) 611–629. doi:10.1038/nrclinonc.2017.44. [PubMed: 28397828]

[23]. Thiery JP, Sleeman JP, Complex networks orchestrate epithelial-mesenchymal transitions, Nat. Rev. Mol. Cell Biol 7 (2006) 131–142. doi:10.1038/nrm1835. [PubMed: 16493418]

[24]. Mathias RA, Wang B, Ji H, Kapp EA, Moritz RL, Zhu HJ, Simpson RJ, Secretome-based proteomic profiling of Ras-transformed MDCK cells reveals extracellular modulators of epithelial-mesenchymal transition, J. Proteome Res 8 (2009) 2827–2837. doi:10.1021/pr8010974. [PubMed: 19296674]

[25]. Scheel C, Eaton EN, Li SHJ, Chaffer CL, Reinhardt F, Kah KJ, Bell G, Guo W, Rubin J, Richardson AL, Weinberg RA, Paracrine and autocrine signals induce and maintain mesenchymal and stem cell states in the breast, Cell. 145 (2011) 926–940. doi:10.1016/j.cell.2011.04.029. [PubMed: 21663795]

[26]. Palena C, Hamilton DH, Fernando RI, NIH Public Access, Futur. Oncol 8 (2013) 713–722. doi:10.2217/fon.12.59.Influence.

[27]. Esquivel-Velázquez M, Ostoa-Saloma P, Palacios-Arreola MI, Nava-Castro KE, Castro JI, Morales-Montor J, The Role of Cytokines in Breast Cancer Development and Progression, J. Interf. Cytokine Res 35 (2015) 1–16. doi:10.1089/jir.2014.0026.

[28]. Snoussi K, Mahfoudh W, Bouaouina N, Ben Ahmed S, Helal AN, Chouchane L, Genetic Variation in IL-8 Associated with Increased Risk and Poor Prognosis of Breast Carcinoma, Hum. Immunol 67 (2006) 13–21. doi:10.1016/j.humimm.2006.03.018. [PubMed: 16698420]

[29]. Reen ARG, Reen VLG, Hite MCW, Peirs VS, Expression of Cytokine Messenger Rna in Normal and Neoplastic Human Breast Tissue : Identification of Interleukin-8 As a Potential Regulatory Factor in Breast Tumours, 941 (1997) 937–941.

[30]. Benoy IH, Salgado R, Van Dam P, Geboers K, Van Marck E, Scharpé S, Vermeulen PB, Dirix LY, Increased serum interleukin-8 in patients with early and metastatic breast cancer correlates with early dissemination and survival, Clin. Cancer Res 10 (2004) 7157–7162. doi:10.1158/1078-0432.CCR-04-0812. [PubMed: 15534087]

[31]. Fernando RI, Castillo MD, Litzinger M, Hamilton DH, Palena C, IL-8 signaling plays a critical role in the epithelial-mesenchymal transition of human carcinoma cells, Cancer Res. 71 (2011) 5296–5306. doi:10.1158/0008-5472.CAN-11-0156. [PubMed: 21653678]

[32]. Yao C, Lin Y, Chua MS, Ye CS, Bi J, Li W, Zhu YF, Wang SM, Interleukin-8 modulates growth and invasiveness of estrogen receptor-negative breast cancer cells, Int. J. Cancer 121 (2007) 1949–1957. doi:10.1002/ijc.22930. [PubMed: 17621625]

[33]. Lin Y, Huang R, Chen L, Li S, Shi Q, Jordan C, Huang RP, Identification of interleukin-8 as estrogen receptor-regulated factor involved in breast cancer invasion and angiogenesis by protein arrays, Int. J. Cancer 109 (2004) 507–515. doi:10.1002/ijc.11724. [PubMed: 14991571]

[34]. Fischbach C, Chen R, Matsumoto T, Schmelzle T, Brugge JS, Polverini PJ, Mooney DJ, Engineering tumors with 3D scaffolds, Nat. Methods 4 (2007) 855–860. doi:10.1038/nmeth1085. [PubMed: 17767164]

[35]. Infanger DW, Lynch ME, Fischbach C, Engineered Culture Models for Studies of Tumor-Microenvironment Interactions, Annu. Rev. Biomed. Eng 15 (2013) 29–53. doi:10.1146/annurev-bioeng-071811-150028. [PubMed: 23642249]

[36]. He J, Genetos DC, Leach JK, Osteogenesis and Trophic Factor Secretion are Influenced by the Composition of Hydroxyapatite/Poly(Lactide-Co-Glycolide) Composite Scaffolds, Tissue Eng. Part A 16 (2010) 127–137. doi:10.1089/ten.tea.2009.0255. [PubMed: 19642853]

[37]. Kim SS, Sun Park M, Jeon O, Yong Choi C, Kim BS, Poly(lactide-co-glycolide)/hydroxyapatite composite scaffolds for bone tissue engineering, Biomaterials. 27 (2006) 1399–1409. doi:10.1016/j.biomaterials.2005.08.016. [PubMed: 16169074]

[38]. Schmittgen TD, Livak KJ, Analyzing real-time PCR data by the comparative CT method, Nat. Protoc 3 (2008) 1101–1108. doi:10.1038/nprot.2008.73. [PubMed: 18546601]

[39]. Lynch ME, Chiou AE, Lee MJ, Marcott SC, Polamraju PV, Lee Y, Fischbach C, Three-Dimensional Mechanical Loading Modulates the Osteogenic Response of Mesenchymal Stem Cells to Tumor-Derived Soluble Signals, Tissue Eng. Part A 22 (2016) 1006–1015. doi:10.1089/ten.tea.2016.0153. [PubMed: 27401765]

[40]. Choi S, Friedrichs J, Song YH, Werner C, Estroff LA, Fischbach C, Intrafibrillar, bone-mimetic collagen mineralization regulates breast cancer cell adhesion and migration, Biomaterials. 10 (2018) 1–12. doi:10.1016/j.biomaterials.2018.05.002.

[41]. So JY, Lee HJ, Kramata P, Minden A, Suh N, Differential Expression of Key Signaling Proteins in MCF10 Cell Lines, a Human Breast Cancer Progression Model., Mol. Cell. Pharmacol 4 (2012) 31–40. doi:11.4255/mcpharmacol.12.03. [PubMed: 24558516]

[42]. Wu F, Chen W, Gillis B, Fischbach C, Estroff LA, Gourdon D, Protein-crystal interface mediates cell adhesion and proangiogenic secretion, Biomaterials. 116 (2017) 174–185. doi:10.1016/j.biomaterials.2016.11.043. [PubMed: 27940370]

[43]. Hu M, Yao J, Carroll DK, Weremowicz S, Chen H, Carrasco D, Richardson A, Violette S, Nikolskaya T, Nikolsky Y, Bauerlein EL, Hahn WC, Gelman RS, Allred C, Bissell MJ, Schnitt S, Polyak K, Regulation of In Situ to Invasive Breast Carcinoma Transition, Cancer Cell. 13 (2008) 394–406. doi:10.1016/j.ccr.2008.03.007. [PubMed: 18455123]

[44]. Christofori G, New signals from the invasive front, Nature. 441 (2006) 444–450. doi:10.1038/nature04872. [PubMed: 16724056]

[45]. Mogilner A, Keren K, The Shape of Motile Cells, Curr. Biol 19 (2009) R762–R771. doi:10.1016/j.cub.2009.06.053. [PubMed: 19906578]

[46]. Rafelski SM, Theriot JA, Crawling Toward a Unified Model of Cell Motility: Spatial and Temporal Regulation of Actin Dynamics, Annu. Rev. Biochem 73 (2004) 209–239. doi:10.1146/annurev.biochem.73.011303.073844. [PubMed: 15189141]

[47]. Kenny PA, Lee GY, Myers CA, Neve RM, Semeiks JR, Spellman PT, Lorenz K, Lee EH, Barcellos-Hoff MH, Petersen OW, Gray JW, Bissell MJ, The morphologies of breast cancer cell lines in three-dimensional assays correlate with their profiles of gene expression, Mol. Oncol 1 (2007) 84–96. doi:10.1016/j.molonc.2007.02.004. [PubMed: 18516279]

[48]. Lourenço BN, Springer NL, Ferreira D, Oliveira C, Granja PL, Fischbach C, CD44v6 increases gastric cancer malignant phenotype by modulating adipose stromal cell-mediated ECM remodeling, Integr. Biol. (United Kingdom) 10 (2018) 145–158. doi:10.1039/c7ib00179g.

[49]. Infanger DW, Cho Y, Lopez BS, Mohanan S, Liu SC, Gursel D, Boockvar JA, Fischbach C, Glioblastoma stem cells are regulated by interleukin-8 signaling in a tumoral perivascular niche, Cancer Res. 73 (2013) 7079–7089. doi:10.1158/0008-5472.CAN-13-1355. [PubMed: 24121485]

[50]. Erbas B, Provenzano E, Armes J, Gertig D, The natural history of ductal carcinoma in situ of the breast: A review, Breast Cancer Res. Treat 97 (2006) 135–144. doi:10.1007/s10549-005-9101-z. [PubMed: 16319971]

[51]. Freund A, Chauveau C, Brouillet J-P, Lucas A, Lacroix M, Licznar A, Vignon F, Lazennec G, IL-8 expression and its possible relationship with estrogen-receptor-negative status of breast cancer cells, Oncogene. 22 (2003) 256–265. doi:10.1038/sj.onc.1206113. [PubMed: 12527894]

[52]. Charafe-Jauffret E, Ginestier C, Iovino F, Wicinski J, Cervera N, Finetti P, Hur MH, Diebel ME, Monville F, Dutcher J, Brown M, Viens P, Xerri L, Bertucci F, Stassi G, Dontu G, Birnbaum D, Wicha MS, Breast cancer cell lines contain functional cancer stem sells with metastatic capacity

and a distinct molecular signature, Cancer Res. 69 (2009) 1302–1313. doi: 10.1158/0008-5472.CAN-08-2741. [PubMed: 19190339]

[53]. Singh B, Berry JA, Vincent LE, Lucci A, Involvement of IL-8 in COX-2-Mediated Bone Metastases from Breast Cancer, J. Surg. Res 134 (2006) 44–51. doi:10.1016/j.jss.2006.03.018. [PubMed: 16678856]

[54]. De Larco JE, Wuertz BRK, Rosner KA, Erickson SA, Gamache DE, Manivel JC, Furcht LT, A potential role for interleukin-8 in the metastatic phenotype of breast carcinoma cells, Am. J. Pathol 158 (2001) 639–646. doi:10.1016/S0002-9440(10)64005-9. [PubMed: 11159200]

[55]. Fischbach C, Kong HJ, Hsiong SX, Evangelista MB, Yuen W, Mooney DJ, Cancer cell angiogenic capability is regulated by 3D culture and integrin engagement, Proc. Natl. Acad. Sci 106 (2009) 399–404. doi:10.1073/pnas.0808932106. [PubMed: 19126683]

[56]. DelNero P, Lane M, Verbridge SS, Kwee B, Kermani P, Hempstead B, Stroock A, Fischbach C, 3D culture broadly regulates tumor cell hypoxia response and angiogenesis via pro-inflammatory pathways, Biomaterials. 55 (2015) 110–118. doi:10.1016/j.biomaterials.2015.03.035. [PubMed: 25934456]

[57]. Al-Hajj M, Wicha MS, Benito-Hernandez A, Morrison SJ, Clarke MF, Prospective identification of tumorigenic breast cancer cells, Proc. Natl. Acad. Sci 100 (2003) 3983–3988. doi:10.1073/pnas.0530291100. [PubMed: 12629218]

[58]. Singh JK, Simões BM, Howell SJ, Farnie G, Clarke RB, Recent advances reveal IL-8 signaling as a potential key to targeting breast cancer stem cells, Breast Cancer Res. 15 (2013) 1–9. doi: 10.1186/bcr3436.

[59]. Stupack DG, Get a ligand, get a life: integrins, signaling and cell survival, J. Cell Sci 115 (2002) 3729–3738. doi:10.1242/jcs.00071. [PubMed: 12235283]

[60]. Felding-Habermann B, O'Toole TE, Smith JW, Fransvea E, Ruggeri ZM, Ginsberg MH, Hughes PE, Pampori N, Shattil SJ, Saven A, Mueller BM, Integrin activation controls metastasis in human breast cancer, Proc. Natl. Acad. Sci 98 (2001) 1853–1858. doi:10.1073/pnas.98.4.1853. [PubMed: 11172040]

[61]. Lowrie AG, Salter DM, Ross JA, Latent effects of fibronectin, α5β1 integrin, αVβ5 integrin and the cytoskeleton regulate pancreatic carcinoma cell IL-8 secretion, Br. J. Cancer 91 (2004) 1327–1334. doi:10.1038/sj.bjc.6602132. [PubMed: 15354211]

[62]. Danhier F, Le Breton A, Préat V, RGD-based strategies to target alpha(v) beta(3) integrin in cancer therapy and diagnosis, Mol. Pharm 9 (2012) 2961–2973. doi:10.1021/mp3002733. [PubMed: 22967287]

[63]. Lee CY, Huang CY, Chen MY, Lin CY, Hsu HC, Tang CH, IL-8 increases integrin expression and cell motility in human chondrosarcoma cells, J. Cell. Biochem 112 (2011) 2549–2557. doi: 10.1002/jcb.23179. [PubMed: 21590707]

[64]. Kaur H, Mao S, Li Q, Sameni M, Krawetz SA, Sloane BF, Mattingly RR, RNA-Seq of Human Breast Ductal Carcinoma In Situ Models Reveals Aldehyde Dehydrogenase Isoform 5A1 as a Novel Potential Target, PLoS One. 7 (2012). doi:10.1371/journal.pone.0050249.

[65]. Barnabas N, Cohen D, Phenotypic and Molecular Characterization of MCF10DCIS and SUM Breast Cancer Cell Lines, Int. J. Breast Cancer 2013 (2013) 1–16. doi:10.1155/2013/872743.

[66]. Todorović-Raković N, Milovanović J, Interleukin-8 in Breast Cancer Progression, J. Interf. Cytokine Res 33 (2013) 563–570. doi:10.1089/jir.2013.0023.

[67]. Ponta H, Sherman L, Herrlich PA, CD44: From adhesion molecules to signalling regulators, Nat. Rev. Mol. Cell Biol 4 (2003) 33–45. doi:10.1038/nrm1004. [PubMed: 12511867]

[68]. Lee JL, Wang MJ, Sudhir PR, Der Chen G, Chi CW, Chen JY, Osteopontin promotes integrin activation through outside-in and inside-out mechanisms: OPN-CD44 V interaction enhances survival in gastrointestinal cancer cells, Cancer Res. 67 (2007) 2089–2097. doi: 10.1158/0008-5472.CAN-06-3625. [PubMed: 17332338]

[69]. Shevde LA, Metge BJ, Mitra A, Xi Y, Ju J, King JA, Samant RS, Spheroid-forming subpopulation of breast cancer cells demonstrates vasculogenic mimicry via hsa-miR-299-5p regulated de novo expression of osteopontin, J. Cell. Mol. Med 14 (2010) 1693–1706. doi: 10.1111/j.1582-4934.2009.00821.x. [PubMed: 19538464]

[70]. Goldberg HA, Warner KJ, Li MC, Hunter GK, Binding of bone sialoprotein, osteopontin and synthetic polypeptides to hydroxyapatite, Connect. Tissue Res 42 (2001) 25–37. doi: 10.3109/03008200109014246. [PubMed: 11696986]

[71]. Bonfiglio R, Scimeca M, Toschi N, Pistolese CA, Giannini E, Antonacci C, Ciuffa S, Tancredi V, Tarantino U, Albonici L, Bonanno E, Radiological, Histological and Chemical Analysis of Breast Microcalcifications: Diagnostic Value and Biological Significance, J. Mammary Gland Biol. Neoplasia 23 (2018) 89–99. doi:10.1007/s10911-018-9396-0. [PubMed: 29744755]

[72]. Rizwan A, Paidi SK, Zheng C, Cheng M, Barman I, Glunde K, Mapping the genetic basis of breast microcalcifications and their role in metastasis, Sci. Rep 8 (2018) 1–10. doi:10.1038/s41598-018-29330-9. [PubMed: 29311619]

[73]. Friedl P, Wolf K, Plasticity of cell migration: A multiscale tuning model, J. Cell Biol 188 (2010) 11–19. doi:10.1083/jcb.200909003. [PubMed: 19951899]

[74]. Paňková K, Rösel D, Novotný M, Brábek J, The molecular mechanisms of transition between mesenchymal and amoeboid invasiveness in tumor cells, Cell. Mol. Life Sci 67 (2010) 63–71. doi:10.1007/s00018-009-0132-1. [PubMed: 19707854]

[75]. Wu PH, Phillip JM, Khatau SB, Chen WC, Stirman J, Rosseel S, Tschudi K, Van Patten J, Wong M, Gupta S, Baras AS, Leek JT, Maitra A, Wirtz D, Evolution of cellular morpho-phenotypes in cancer metastasis, Sci. Rep 5 (2015) 1–10. doi:10.1038/srep18437.

[76]. Li A, Varney ML, Valasek J, Godfrey M, Dave BJ, Singh RK, Autocrine role of interleukin-8 in induction of endothelial cell proliferation, survival, migration and MMP-2 production and angiogenesis, Angiogenesis. 8 (2005) 63–71. doi:10.1007/s10456-005-5208-4. [PubMed: 16132619]

[77]. Li XJ, Peng LX, Shao JY, Lu WH, Zhang JX, Chen S, Chen ZY, Xiang YQ, Bao YN, Zheng FJ, Zeng MS, Kang TB, Zeng YX, Teh BT, Qian CN, As an independent unfavorable prognostic factor, IL-8 promotes metastasis of nasopharyngeal carcinoma through induction of epithelial-mesenchymal transition and activation of AKT signaling, Carcinogenesis. 33 (2012) 1302–1309. doi:10.1093/carcin/bgs181. [PubMed: 22610073]

[78]. Araki K, Shimura T, Yajima T, Tsutsumi S, Suzuki H, Okada K, Kobayashi T, Raz A, Kuwano H, Phosphoglucose isomerase/autocrine motility factor promotes melanoma cell migration through ERK activation dependent on autocrine production of interleukin-8, J. Biol. Chem 284 (2009) 32305–32311. doi:10.1074/jbc.M109.008250. [PubMed: 19801670]

[79]. Jayatilaka H, Tyle P, Chen JJ, Kwak M, Ju J, Kim HJ, Lee JSH, Wu PH, Gilkes DM, Fan R, Wirtz D, Synergistic IL-6 and IL-8 paracrine signalling pathway infers a strategy to inhibit tumour cell migration, Nat. Commun 8 (2017) 1–12. doi:10.1038/ncomms15584. [PubMed: 28232747]

[80]. Cox RF, Morgan MP, Microcalcifications in breast cancer: Lessons from physiological mineralization, Bone. 53 (2013) 437–450. doi:10.1016/j.bone.2013.01.013. [PubMed: 23334083]

[81]. Scimeca M, Antonacci C, Toschi N, Giannini E, Bonfiglio R, Buonomo CO, Pistolese CA, Tarantino U, Bonanno E, Breast Osteoblast-like Cells: A Reliable Early Marker for Bone Metastases From Breast Cancer, Clin. Breast Cancer 18 (2018) e659–e669. doi:10.1016/j.clbc.2017.11.020. [PubMed: 29306659]

[82]. Karnoub AE, Dash AB, Vo AP, Sullivan A, Brooks MW, Bell GW, Richardson AL, Polyak K, Tubo R, Weinberg RA, Mesenchymal stem cells within tumour stroma promote breast cancer metastasis, Nature. 449 (2007) 557–563. doi:10.1038/nature06188. [PubMed: 17914389]

[83]. Yoon Y-S, Unexpected Severe Calcification After Transplantation of Bone Marrow Cells in Acute Myocardial Infarction, Circulation. 109 (2004) 3154–3157. doi:10.1161/01.CIR.0000134696.08436.65. [PubMed: 15197139]

[84]. Breitbach M, Bostani T, Roell W, Xia Y, Dewald O, Nygren JM, Fries JWU, Tiemann K, Bohlen H, Hescheler J, Welz A, Bloch W, Jacobsen SEW, Potential risks of bone marrow cell transplantation into infarcted hearts, Hematology. 110 (2007) 1362–1369. doi:10.1182/blood-2006-12-063412.The.

[85]. Cowell CF, Weigelt B, Sakr RA, Ng CKY, Hicks J, King TA, Reis-Filho JS, Progression from ductal carcinoma in situ to invasive breast cancer: Revisited, Mol. Oncol 7 (2013) 859–869. doi:10.1016/j.molonc.2013.07.005. [PubMed: 23890733]

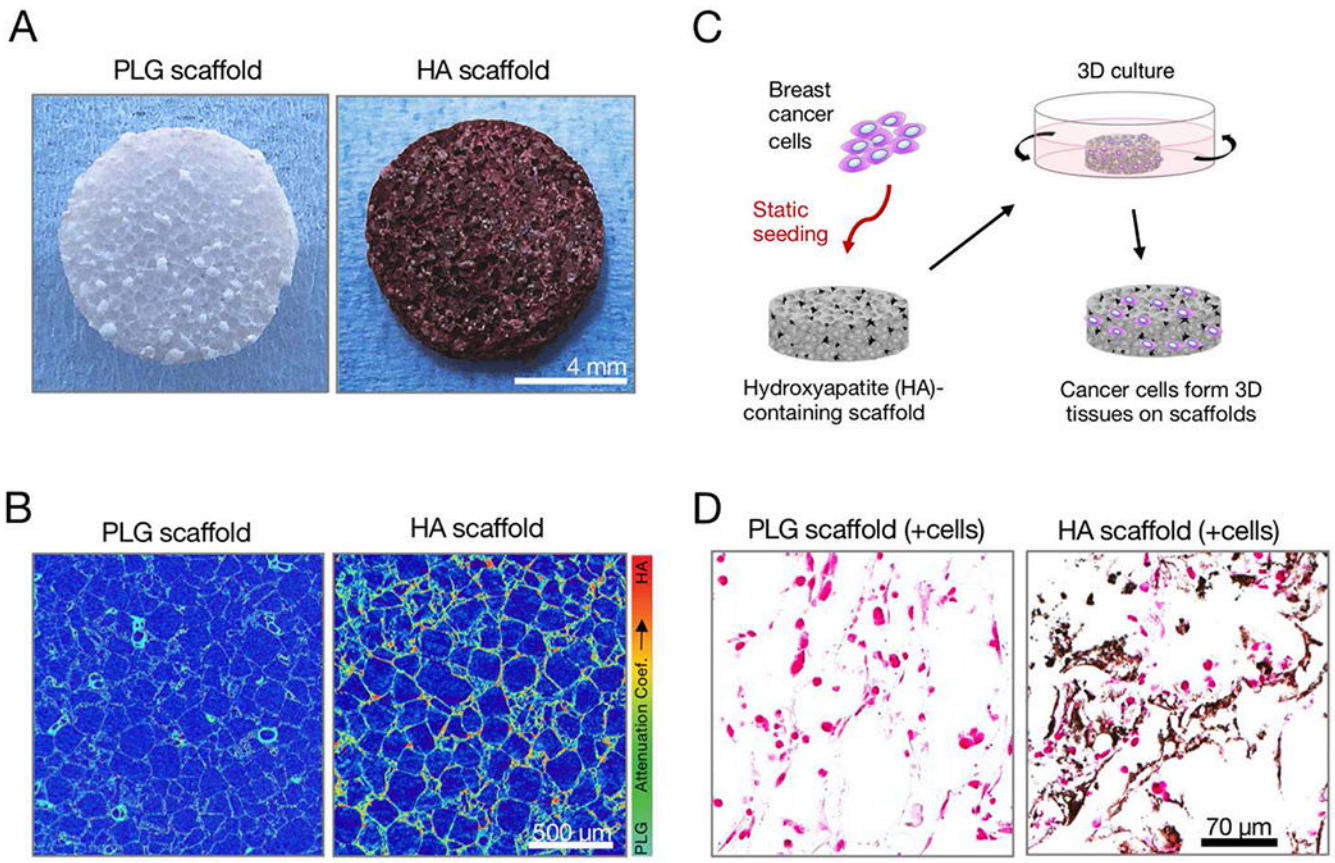

Fig. 1. Hydroxyapatite-containing PLG scaffolds enable study of cell-mineral interactions in 3D.

(**A**) Representative Alizarin Red S stain showing surface presentation of mineral in hydroxyapatite (HA)-containing scaffolds versus PLG control scaffolds. (**B**) Representative false-color microCT cross-sections showing mineral distribution as a function of the attenuation coefficient, which increases with atomic number. (**C**) Setup of 3D culture system: breast cancer cells were statically seeded onto HA-containing PLG scaffolds and then maintained under dynamic culture conditions on an orbital shaker. (**D**) Representative Von Kossa-stained histological cross-sections showing both calcium phosphate mineral (black) and cell nuclei (pink) in tumor cell-seeded HA scaffolds versus tumor cell-seeded PLG scaffolds.

A

ID	Pathology	MCs	Presentation	IL-8	Age	Meno.	BMI	ER	PR	HER2
1	DCIS/IDC	N	No suspicious microcalcifications	0	50	Pre	27.53	Pos	Pos	Neg
2	DCIS/LCIS/IDC	N	No description available	2	71	Post	33.46	Pos	Pos	Neg
3	DCIS/IDC	N	None identified	2	51	Pre	22.36	Neg	Pos	Neg
4	DCIS/LCIS/IDC	N	None identified	0	53	Post	29.37	Pos	Pos	Neg
5	DCIS/IDC	N	No description available	2	64	Post	27.30	Pos	Pos	Neg
6	DCIS/IDC	N	None identified	2	47	Pre	28.10	Pos	Pos	Neg
7	DCIS/IDC	N	None identified	1	83	Post	24.36	Pos	Pos	Neg
8	DCIS/IDC/ILC	Y	Pleomorphic calcifications in segmental distribution	2	57	Post	30.35	Pos	Neg	Pos
9	DCIS/IDC	Y	Malignant pleomorphic calcifications	3	47	Pre	23.78	Pos	Pos	Neg
10	DCIS/LCIS/IDC	Y	Pleomorphic calcifications	3	60	Post	23.49	Neg	Neg	Pos
11	DCIS/IDC	Y	Pleomorphic microcalcifications	2	50	Post	28.35	Pos	Neg	Pos
12	DCIS/IDC	Y	Pleomorphic calcifications considered to be indeterminate	2	57	Post	23.46	Neg	Neg	Pos
13	DCIS/IDC	Y	Extensive heterogeneous and pleomorphic calcifications, cross the midline medially	2	26	Pre	19.61	Pos	Pos	Neg
14	DCIS/IDC	Y	Pleomorphic calcifications	2	44	Pre	23.32	Neg	Neg	Pos
15	DCIS/IDC	Y	Associated microcalcifications	1	62	Post	34.31	Neg	Neg	Pos
16	DCIS/IDC	Y	Amorphous calcifications	3	40	Pre	26.40	Neg	Neg	Neg

Notable abbreviations: 'DCIS' – ductal carcinoma *in situ*; 'IDC' – invasive ductal carcinoma; 'LCIS' – lobular carcinoma *in situ*; 'ILC' – invasive lobular carcinoma; 'MCs' – mammographic calcifications; 'IL-8' – total IL-8 immunohistochemistry score; 'Meno.' - menopause

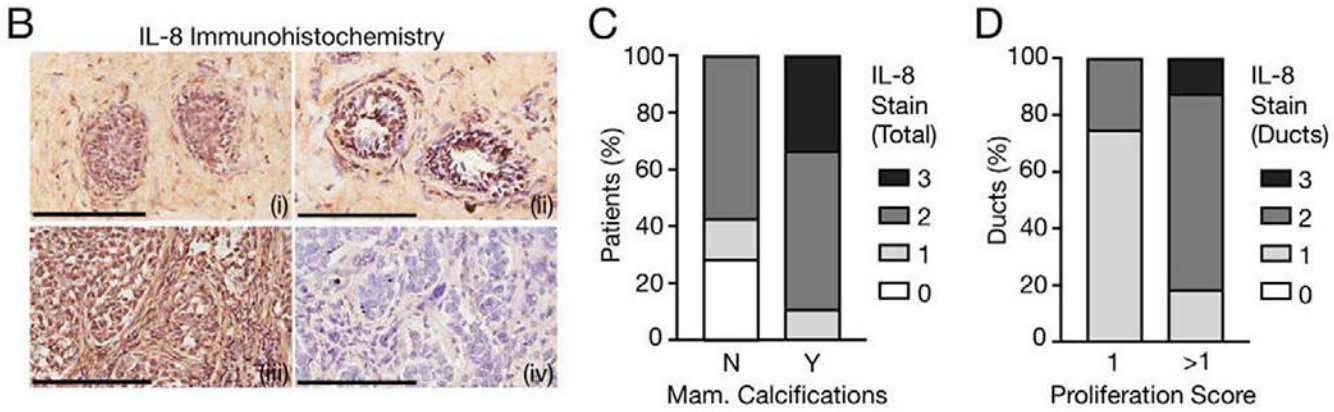

Fig. 2. Histopathological analysis of human breast cancer samples correlates IL-8 enrichment with the presence of mammographic calcifications and proliferative ductal epithelia.

(**A**) Patient information for assessed specimens, sorted by presence of mammographic calcifications. 'IL-8' indicates the corresponding degree of total IL-8 stain via immunohistochemistry (IHC). This chart represents an expanded version of a previously published dataset [5]. (**B**) Representative IL-8 IHC with hematoxylin counterstain. Image labels: (i) - Weak ductal; (ii) - Strong ductal; (iii) - Strong ductal and stromal; (iv) – No IgG. Scale bars, 200 μm. (**C**) Histopathological scoring for the degree of total IL-8 stain as a function of mammographic calcifications. Rubric for total IL-8 staining intensity: 0-to-3, with 0 representing negligible intensity and 3 representing maximum staining. N *vs.* Y: $p<0.05$. (**D**) Histopathological scoring for the degree of ductal IL-8 stain as a function of the ductal proliferation score. Rubric for ductal IL-8 staining intensity: 0-to-3, with 0 representing negligible intensity and 3 representing maximum staining. Rubric for ductal proliferation: 0-to-3, with 0 representing negligible proliferation and 3 representing excessive proliferation and total deterioration of acinar architecture. 1 *vs.* >1: $p<0.05$.

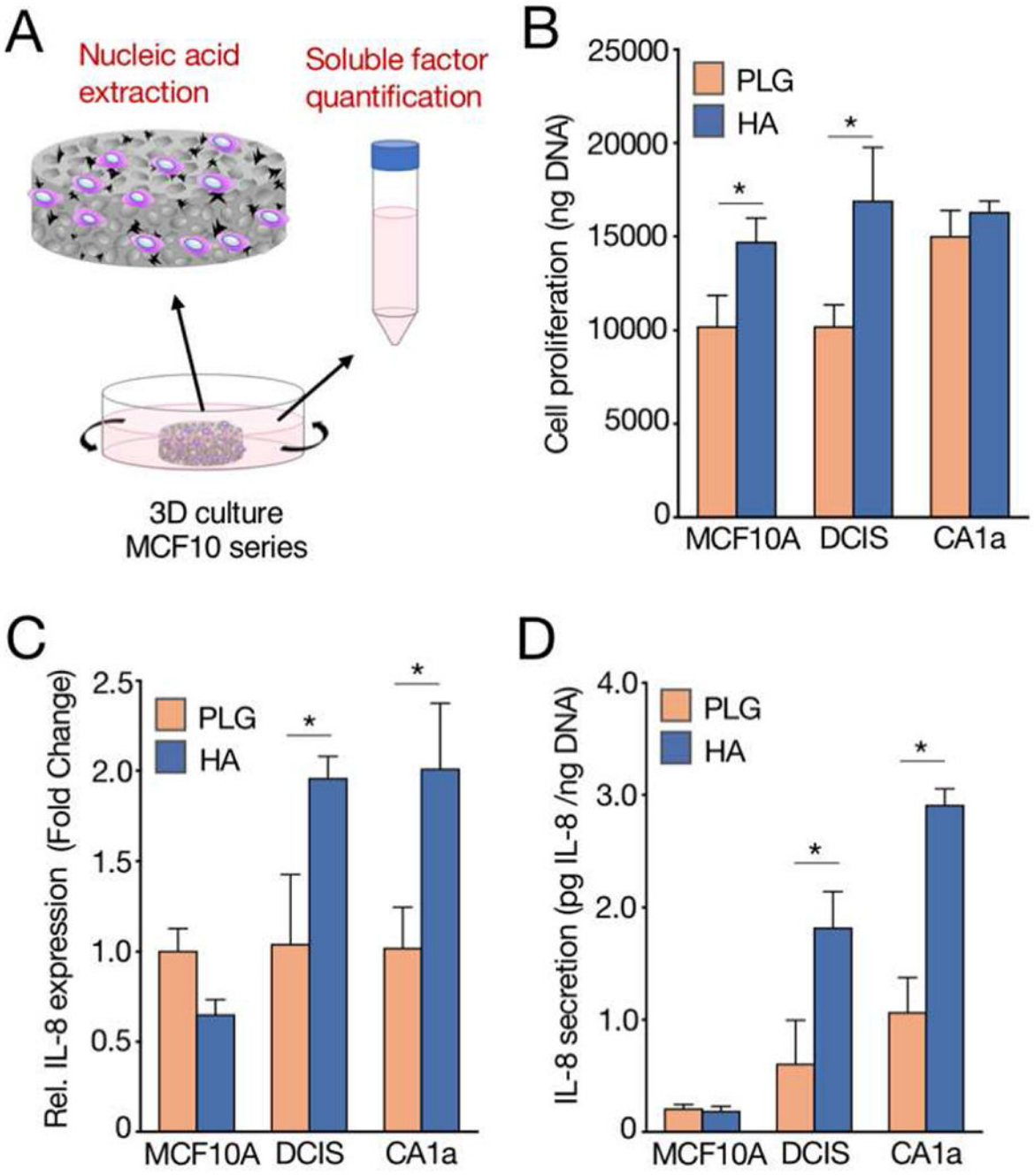

Fig. 3. Hydroxyapatite mineral regulates breast cancer cell proliferation and IL-8 secretion based on malignancy

(**A**) Schematic showing extraction of nucleic acids and quantification of soluble factors from 3D cultures of MCF10 series-seeded scaffolds. (**B**) Fluorimetric quantification of DNA harvested from breast cancer cell lines cultured in scaffolds. (**C**) qRT-PCR analysis of IL-8 gene expression from RNA harvested from breast cancer cell lines cultured in scaffolds. (**D**) Levels of secreted IL-8 in tumor-conditioned media as quantified by ELISA and normalized to fluorimetrically-determined DNA content. Data are means +/− SD. For all plots, *p<0.05.

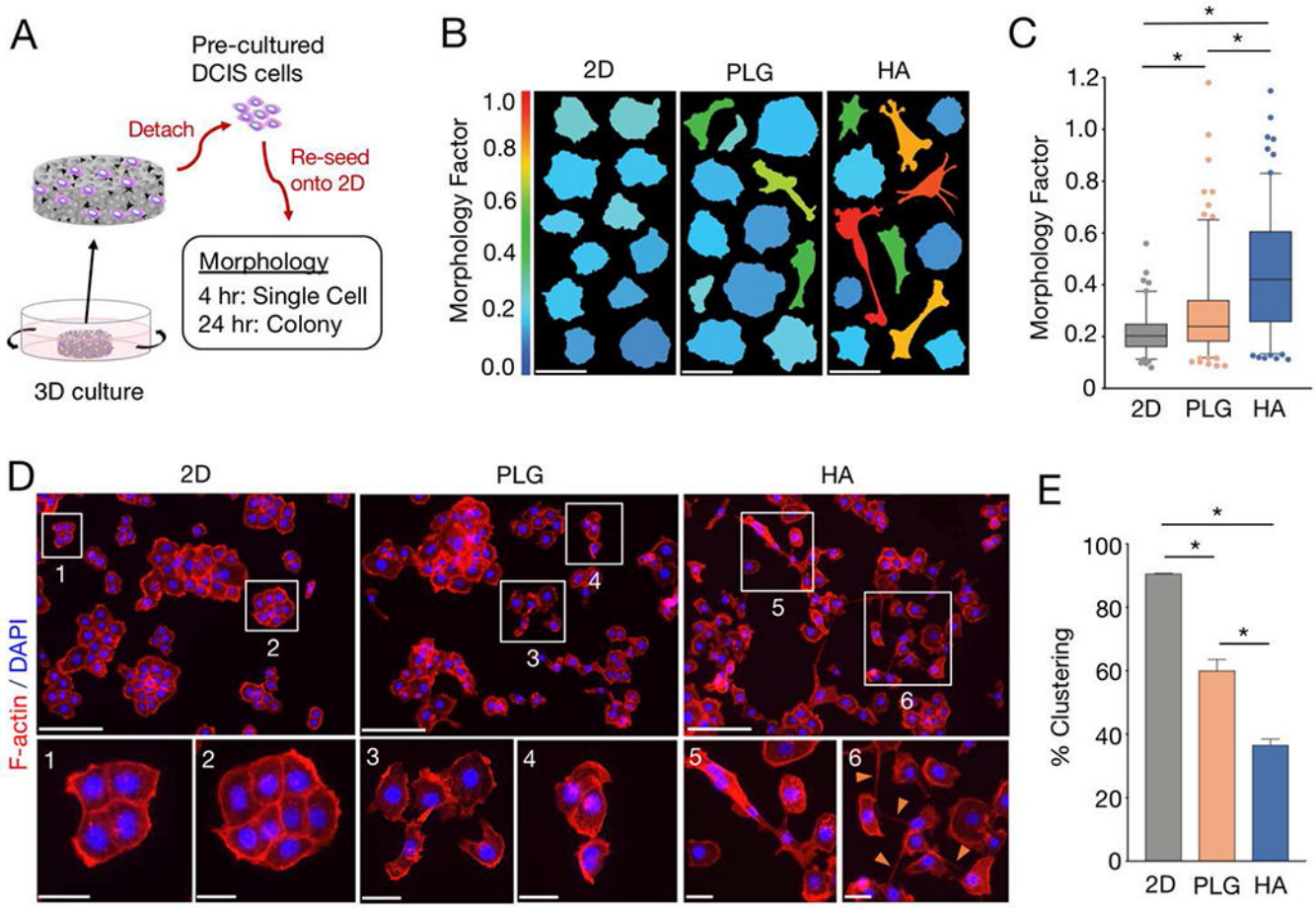

Fig. 4. DCIS cells interacting with hydroxyapatite mineral in 3D culture adopt morphological hallmarks of invasiveness.

(**A**) Experimental setup for morphological characterization: pre-cultured MCF10DCIS.com (DCIS) cells were detached from scaffolds, re-seeded onto fibronectin-coated glass coverslips, and evaluated for single cell (4 hours) and cell colony (24 hours) morphological characteristics. 2D pre-cultures on polystyrene were used as controls. (**B**) Representative cell morphologies of F-actin- and DAPI-stained DCIS cells exposed to different pre-culture conditions. Each vertical panel shows thresholded images of 12 representative cells with a mean Morphology Factor (MF) equivalent to the mean MF of each respective condition. Color scale: warmer colors indicate greater MF. Scale bars, 50 μm. (**C**) Box-and-whisker plots comparing MFs between pre-culture conditions. Whiskers represent the 5th and 95th percentile. Outlier data points are depicted as dots. *p<0.05. (**D**) Representative fluorescent images from DCIS cells exposed to different pre-culture conditions. Cells were co-stained for F-actin (red) and nuclei (blue). Insets magnify the regions outlined by white boxes. Orange arrows in inset 6 highlight cellular processes. Scale bars: top panels, 200 μm; bottom panels, 50 μm. (**E**) Graph comparing % clustering between pre-culture conditions. Data are means +/− SD. *p<0.05.

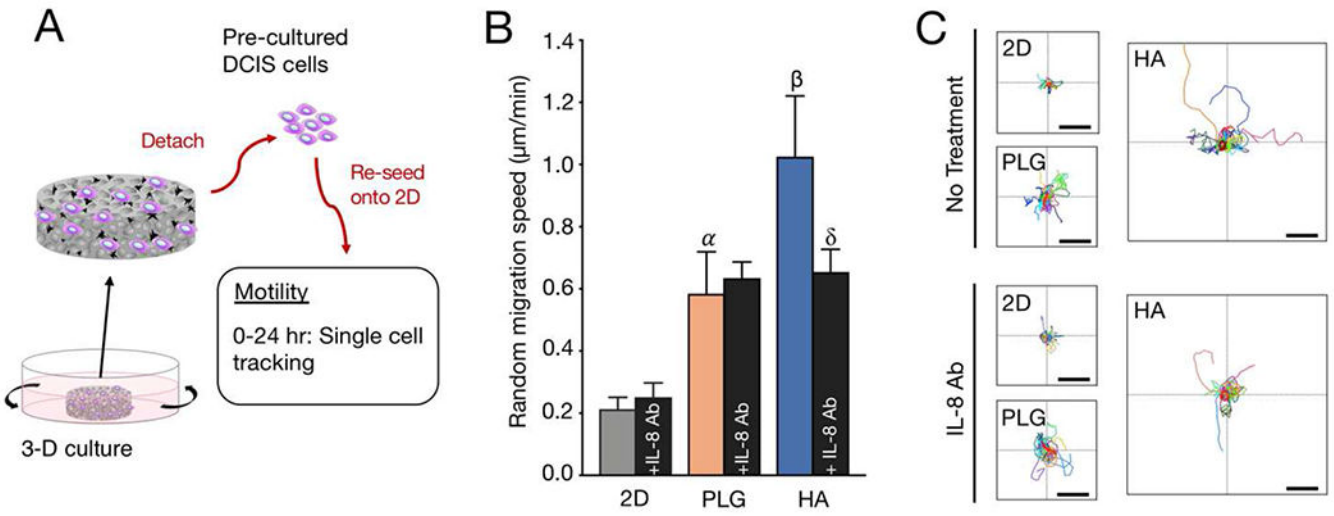

Fig. 5. Hydroxyapatite mineral increases DCIS cell motility through IL-8.

(**A**) Experimental setup for assessment of random migration: pre-cultured MCF10DCIS.com (DCIS) cells were detached from scaffolds, re-seeded onto Fn-coated optically-clear plates, and evaluated for indices of cell motility over 24 hours. In addition to the indicated pre-culture conditions, cells were treated with IL-8 antibody (20 μg/mL) at the start of the tracking period. Cells were analyzed for their x- y- movement over 300-minute timeframes. 2D polystyrene pre-cultures were used as controls. (**B**) Comparison of random migration speeds of cells pre-cultured in different conditions. Data are means +/− SD. α ($p<0.05$): PLG *vs.* 2D. β ($p<0.05$): HA *vs.* PLG; HA *vs.* 2D. δ ($p<0.05$): HA+IL8 Ab *vs.* HA. (**C**) Relative (x, y) trajectories of single cells tracked for 300 minutes from different pre-culture conditions. For each plot, the lines intersect at position (0,0). Scale bars, 100 μm.

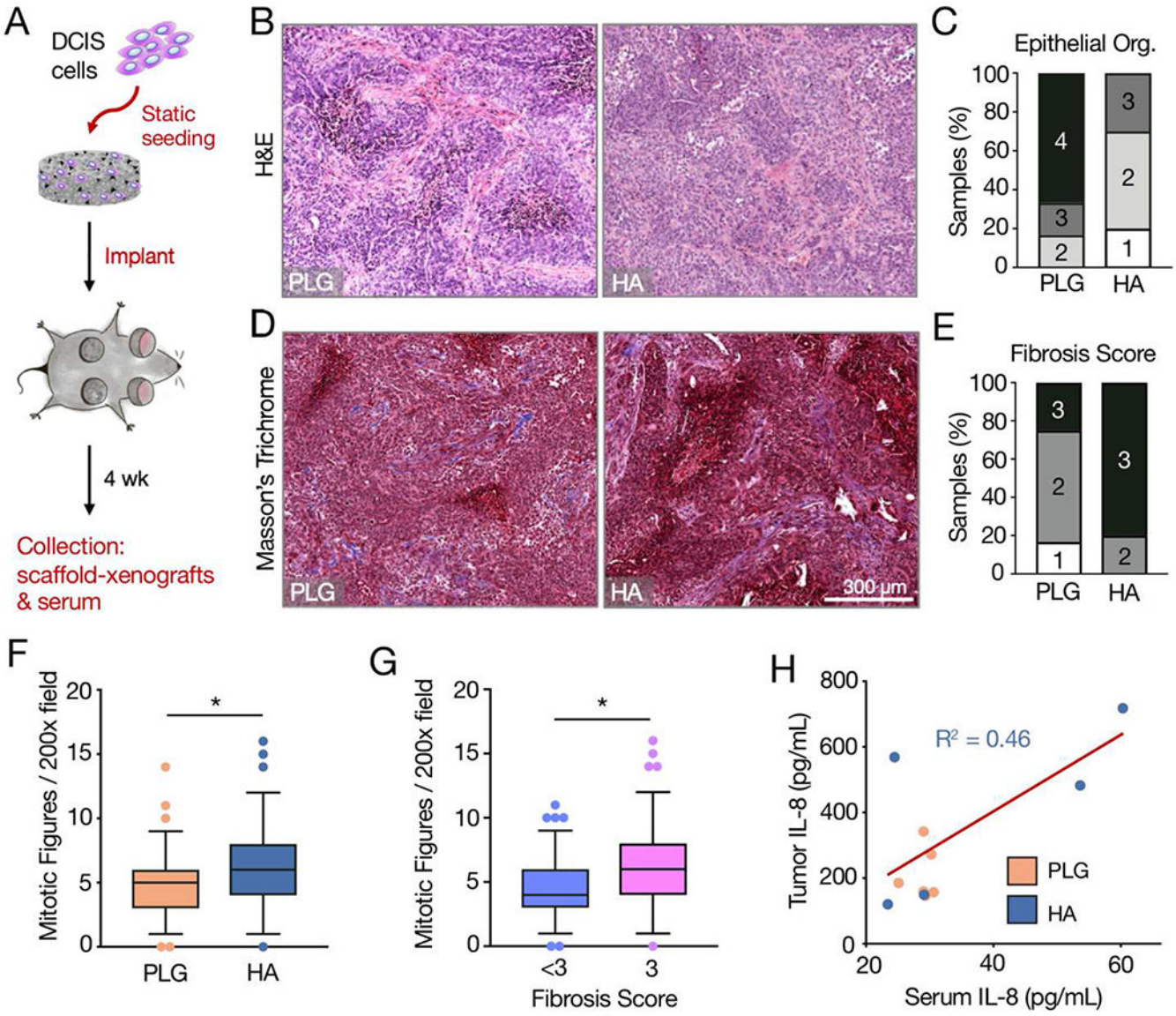

Fig. 6. Exposure of DCIS cells to hydroxyapatite mineral in scaffolds promotes features of increased malignancy *in vivo*.

(**A**) Experimental setup for scaffold-xenograft studies: Mineral-containing or control scaffolds seeded with 0.5e6 MCF10DCIS.com cells were implanted subcutaneously near the third mammary fat pad. Two scaffolds were implanted per animal. After 4 weeks, scaffold-xenograft tumors and serum were collected for histopathological and biochemical analyses. (**B**) Representative hematoxylin and eosin stained cross sections showing epithelial organization. (**C**) Histopathological scoring of the epithelial organization as seen in (B). Rubric: 1-to-4, least-to-most organized, details in methods. PLG *vs.* HA: $p<0.05$. (**D**) Representative Masson's trichrome stained cross sections showing the presence of collagen fibers. (**E**) Histopathological scoring of the fibrosis as seen in (D). Rubric: 1-to-3, least-to-most fibrosis, details in methods. PLG *vs.* HA: $p<0.05$. (**F**) Box-and-whisker plots showing Mitotic Figures (chromosomes in a given 200x field). Whiskers represent the 5th and 95th

percentile. Outlier data points are depicted as dots. (**G**) Box-and-whisker plots showing Mitotic Figures as a function of Fibrosis Score. Whiskers represent the 5^{th} and 95^{th} percentile. Outlier data points are depicted as dots. (**H**) Scatter-plot of serum IL-8 *vs.* tumor IL-8 as detected by ELISA. Correlation as determined by simple linear regression is for HA data points only. For all plots, *$p<0.05$.